

See discussions, stats, and author profiles for this publication at: <https://www.researchgate.net/publication/282027765>

Microstructure Observations of Natural Gas Hydrate Occurrence in Porous Media Using Microfocus X-Ray Computed Tomography

ARTICLE in ENERGY & FUELS · JULY 2015

Impact Factor: 2.79 · DOI: 10.1021/acs.energyfuels.5b00881

READS

49

6 AUTHORS, INCLUDING:



Lei Yang

Dalian University of Technology

10 PUBLICATIONS 28 CITATIONS

[SEE PROFILE](#)



Weiguo Liu

Dalian University of Technology

55 PUBLICATIONS 331 CITATIONS

[SEE PROFILE](#)



Yanghui Li

Yamaguchi University

31 PUBLICATIONS 207 CITATIONS

[SEE PROFILE](#)



Mingjun Yang

Dalian University of Technology

76 PUBLICATIONS 336 CITATIONS

[SEE PROFILE](#)

Microstructure Observations of Natural Gas Hydrate Occurrence in Porous Media Using Microfocus X-ray Computed Tomography

Lei Yang, Jiafei Zhao,* Weiguo Liu, Yanghui Li, Mingjun Yang, and Yongchen Song*

Key Laboratory of Ocean Energy Utilization and Energy Conservation of Ministry of Education, Dalian University of Technology, Dalian, Liaoning 116024, People's Republic of China

ABSTRACT: Natural gas hydrates are globally considered a potential alternative form of energy suitable for sustainable development. The microstructure of natural gas hydrates in sediments governs their seismic and acoustic exploration, stability of seafloors, and gas production from hydrate deposits. To investigate the microstructure and occurrence of natural gas hydrates in pores, natural gas hydrate-bearing porous media were directly observed using microfocus X-ray computed tomography (CT). The spatial distributions of free gas, natural gas hydrates, water, and grains were identified. The results indicated the preference of natural gas hydrates to form primarily within pore spaces and not to cement the adjacent grains, which was described by the floating model. Moreover, the migration of gas and water within pore spaces during hydrate formation appeared random, and natural gas hydrates were found to nucleate preferentially at the gas–water interface. The values of porosity and hydrate saturation obtained via reconstruction of CT images agreed well with the conventional methods, indicating that X-ray CT is effective in microstructural studies on natural gas hydrate-bearing sediments. These findings could have implications for both understanding of natural gas hydrate existence within deposits and future gas production from hydrate-bearing sediments.

Natural gas hydrates are widely regarded as a potential strategic energy form because of their high energy density, purity, and enormous reserves.^{1–5} The microscopic nucleation and formation kinetics of natural gas hydrates in a porous media are of importance to the effective utilization of the huge resources.^{6–9} There are four models for the formation of natural gas hydrates within the pore spaces of hydrate-bearing sediments: floating, supporting, coating, and cementing.^{10,11} The occurrence model and the microstructure of natural gas hydrates within the pores directly govern the mechanical behavior of the sediments, incorporating aspects of solid deformation, multiphase flow, and phase transformation.^{10,12,13} Moreover, the attenuation and transmission of compressional and shear seismic waves during natural gas hydrate exploration are strongly controlled by the spatial distribution of the natural gas hydrates within the pores.^{13–16} On the basis of nuclear magnetic resonance (NMR) relaxation time measurements, Kleinberg et al. found that hydrates tended to replace water in the largest pore spaces but did not coat the grains.¹⁷ Using synchrotron X-ray computed microtomography, Kerkar et al. showed that the nucleation of tetrahydrofuran (THF) hydrates was random and away from grain surfaces.¹⁸ Uchida et al. visually investigated the occurrences of natural gas hydrate at the drill site of Mallik using an X-ray computed tomography (CT) scanner technique.¹⁹ Klapproth et al. reported methane hydrate formation in a gas-saturated porous media using cryogenic scanning electron microscopy (SEM).²⁰ Furthermore, Song et al. discovered that THF hydrate growth was first modeled by the cementing model and then by the floating model, following an increase of the water concentration.^{21,22} THF hydrates are commonly studied as substitutes for natural gas hydrates because of their similar physical properties.^{23–25} However, little research has been performed on the microstructure and occurrence model of gas hydrates, especially methane hydrates, within the pore spaces of porous media.

The X-ray technique is commonly used to obtain three-dimensional (3D) visualizations of a sample nondestructively. Many studies have been conducted regarding the observation of the microstructure of hydrate-bearing sediments.^{26–32} Kneafsey et al. determined local density changes during hydrate formation and dissociation in porous media using X-ray CT.³³ The changes in the distribution of gas hydrates within hydrate-cemented sediments during the depressurization/repressurization process were tracked by Waite et al. using X-ray CT.^{34,35} Furthermore, the dissociation of gas hydrates in core samples collected from Mallik 2L-38 (a gas hydrate research well drilled in Canada) was observed using X-ray CT by Mikami et al.³⁶ Additionally, the structure of gas hydrate-bearing sediments was characterized using microfocus X-ray CT by Jin et al.^{37,38} Synchrotron radiation X-ray cryotomographic microscopy is also employed for the 3D microstructure analyses of natural gas hydrate samples.^{39,40} However, studies on the morphological microstructure and occurrence pattern of natural gas hydrates within pore spaces have not been previously reported.

In the present study, a microfocus X-ray CT (SMX-225CTX-SV, Shimadzu Co., Japan) experimental system was established for the observation of microstructure and occurrence of natural gas hydrates in porous media, as shown in Figure 1. This CT apparatus can attain a maximum resolution as high as 4 μm/pixel. A pressure vessel made of polyimide with an inner diameter of 10 mm and a wall thickness of 8 mm was used to form the natural gas hydrates. Quartz glass sands (AS-ONE, Co., Japan) BZ-1 with an average grain diameter of 1.19 mm were employed to simulate the porous media. The pore

Received: April 21, 2015

Revised: July 16, 2015

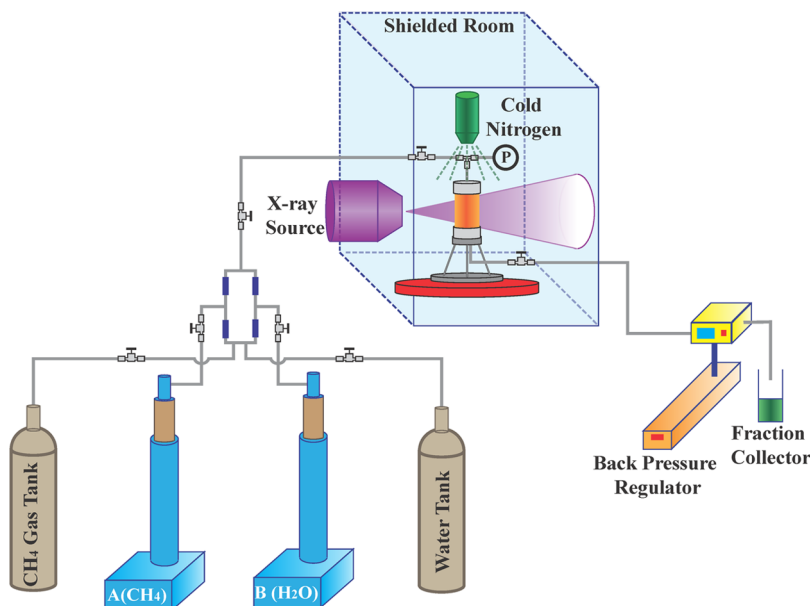


Figure 1. Schematic of the experimental apparatus used in this study.

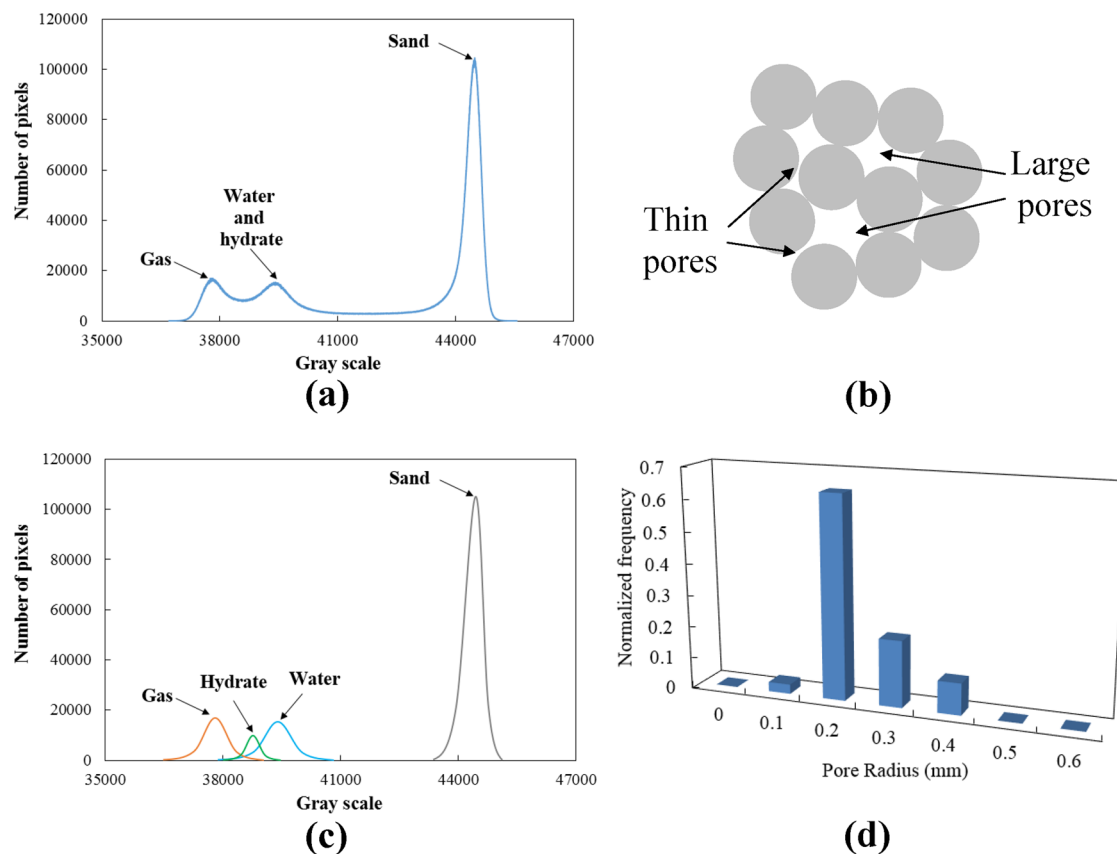


Figure 2. Gray-scale analysis of CT images and pore structure of silica sands.

morphology is described by the combination of round and thin pores, as shown in Figure 2b. The average and maximum pore radius are 0.234 and 0.512 mm; the average and maximum throat radius are 0.126 and 0.422 mm; and the average and maximum coordination numbers are 6.34 and 20. The pore radius distribution is shown in Figure 2d. To observe the microstructural characteristics of natural gas hydrates in pores better, large grains were used. The findings in large pores would

have implications for the actual distribution of gas hydrates in natural deposits. The deionized water of 0.15 mL was injected into the porous media, saturated with methane gas (99.99% purity) at an initial pressure of 7 MPa. The pressure vessel was immersed in a water bath at 1 °C for hydrate formation. The temperature–pressure conditions are favorable for hydrate formation without water freezing. A sharp pressure drop indicated the initial formation of natural gas hydrates, and the

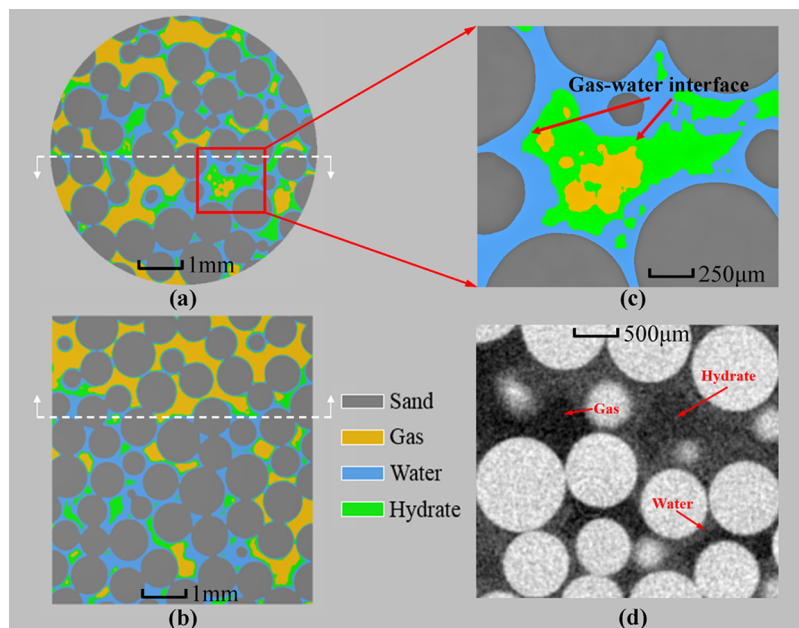


Figure 3. Original local 2D gray-scale image and processed reconstruction image of natural gas hydrate-bearing sands. The component in green represents the hydrate phase, which has no contact with the grain surfaces. The water layer in blue was observed to coat the sands.

entire growth process was considered complete when the pressure became constant again.^{41,42} Then, with cold nitrogen blowing on it to prevent hydrate dissociation, the vessel was placed on the precision rotation stage for CT scanning. A metal bracket was used to fix the sample on the stage, and a locating pin under the holder prevented the relative motion between the holder and the stage to ensure the image quality. The CT imaging was performed at a source voltage of 80 kV and a current of 40 μ A. A full-scan mode with 1200 number of views, 8 average counts, a source object distance (SOD) of 65.7 mm, and a source image distance (SID) of 800.0 mm was used. A 3D image was acquired after the stage rotated through 360° in 320 s. The images were obtained with a 16-bit gray scale and 512 \times 512 pixel resolution. The distance between image slices is 25 μ m. The field of view (FOV) covers a majority of the vessel, and we focus on the top part of the sediments, where gas and water are injected and most hydrates are formed. The image processing software ImageJ and VGStudio MAX were used to process and analyze the CT images.⁴³ Because the process of gas hydrate crystal growth was random, repeated trials were conducted.

Figure 3d shows the original local two-dimensional (2D) CT gray-scale image of natural gas hydrate-bearing sediments. The different gray scales in the CT image reflect the different attenuation coefficients of X-rays, which are determined directly by the density of each component of the sediments. Therefore, sands with higher density are shown to be much brighter in the image than gases. However, considering the relatively small density difference between the natural gas hydrates (0.91 g/cm³) and water,³⁸ the image processing software ImageJ and VGStudio MAX were used to analyze the gray-scale information in the CT images. On the basis of the work of Jin and Sato et al.,^{37,38,44} the gray-scale range was segmented into four sections depending upon the densities of the four components in the sample, as shown in panels a and c of Figure 2. The reconstruction images were processed according to the gray-scale segmentation. The processed cross- and longitudinal sections of the reconstruction image of natural gas hydrate-

bearing sands are illustrated in panels a–c of Figure 3. The free gas, natural gas hydrates, and water within the pore spaces can be clearly differentiated, and thus, their spatial distributions can be determined. As shown, each component is distributed randomly within the pores; however, in Figure 3b, large amounts of free methane gas can be observed to have accumulated on the top of the sediments, indicating that a free gas layer existed and that it was difficult for the methane gas to dissolve and diffuse into pore water to form hydrates. Because of the capillary force and surface wettability of grains, a very thin water layer coated the surfaces of the grains on the top of the sediments. A small quantity of natural gas hydrates formed at the gas–water interface, resulting in very low hydrate saturation. Therefore, the low solubility and diffusivity of methane gas into the pore water and the low water saturation in the free gas layer are considered the main obstacles to the formation of natural gas hydrates with high saturation; i.e., sufficient contact area between the methane gas and water is necessary for hydrate formation. Moreover, the migration of pore water, diffusion of the free gas, and nucleation locations of the natural gas hydrates were random. According to Figure 3c, natural gas hydrates were observed to occur primarily within the pores of sediments rather than tightly cementing the adjacent grains, which was identified as the free-floating model. A water layer existed between the natural gas hydrates and the grains, confirming that natural gas hydrates did not nucleate and grow at the surface of the substrate. It also showed that natural gas hydrates formed at the interface of methane gas and pore water, where the guest molecules and water framework coexisted, making it suitable for the initial crystal growth of natural gas hydrates. However, free gas could occur in the middle of the area with concentrated hydrate formation, as shown in Figure 3c. This could be attributed to the fact that the formation of natural gas hydrates prevented further contact between methane gas and water, thereby delaying the further formation of natural gas hydrates. In addition, the lack of an interface between gas and water within the sediments indicated the completion of natural gas hydrate synthesis. Thus, it was

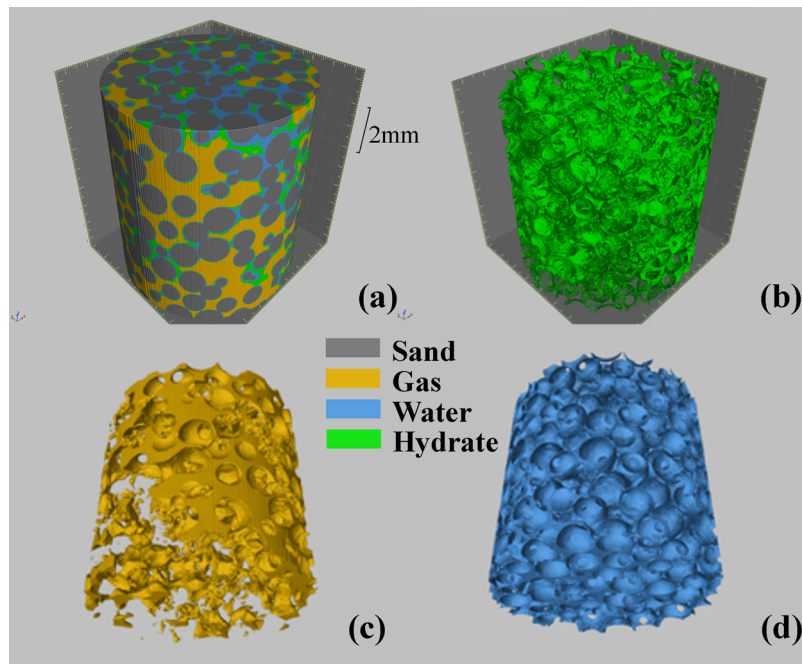


Figure 4. Three-dimensional reconstruction images of natural gas hydrate-bearing sediments and each component. Gases were non-uniformly distributed in the pores, which contributed to lower saturation of natural gas hydrates in the bottom part.

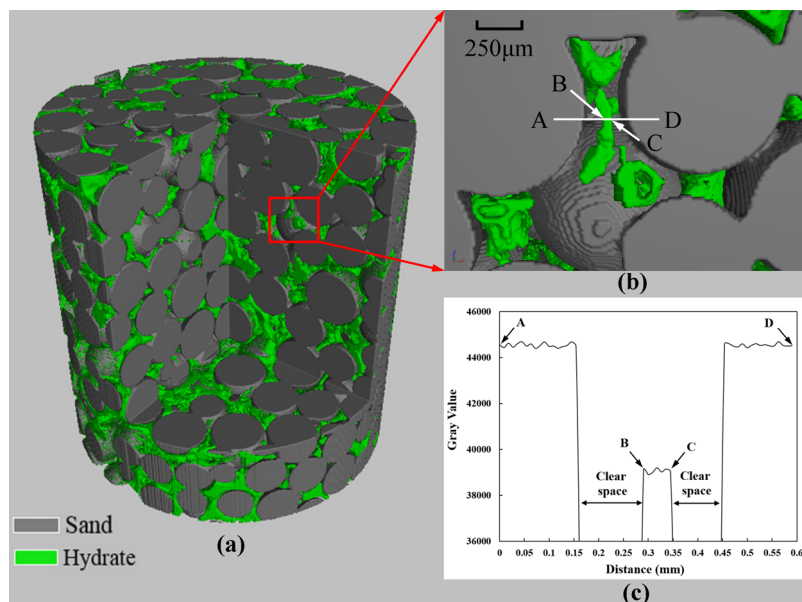


Figure 5. Spatial occurrence and gray-scale distribution of the hydrate phase in the pores. There existed clear spaces between natural gas hydrates and grain surfaces.

further confirmed that sufficient contact between the guest molecules and water framework is essential for hydrate formation. Therefore, the growth process of natural gas hydrates in sediments was initiated within pore spaces at the gas–water interface, where hydrate crystals nucleated. Then, natural gas hydrates gradually grew and accumulated but did not contact the surrounding grains. The formation of natural gas hydrates restricted the contact between water and gas, preventing further hydrate formation. Finally, the formation process of natural gas hydrates was considered complete when an interface between methane gas and water no longer existed.

The 3D reconstruction images of the natural gas hydrate-bearing sediments and each component are presented in Figure

4. Information on each slice of the sediments can be obtained from the reconstruction images, and furthermore, the morphological and geometric properties of the complete sediments and of each component can be derived. Thus, the porosity of the sediments was calculated to be 39.8% by acquiring the volume information on pores and complete sediments. This value is comparable to that obtained by the water injection method (40.0%). Moreover, the saturation of natural gas hydrates, which is defined as the volume fraction of natural gas hydrates to the entire pore volume, was determined to be 19.8% by obtaining the volumes of natural gas hydrates and pores. On the basis of the data acquisition system, the saturation of natural gas hydrates can be calculated using the

Peng–Robinson equation of state.^{45–47} The pore volume is equal to the total volume of initial methane gas (V_g) and water (V_w) before hydrate formation and the volume of residual gas (V_{rg}), residual water (V_{rw}), and natural gas hydrates (V_h) after hydrate formation. We assumed that the hydration number of natural gas hydrates is 5.75, the density of natural gas hydrates is 0.91 g/cm³, and water is incompressible.¹² The volume and mole number of methane gas can be obtained using the Peng–Robinson equation of state, which can be expressed as follows:

$$P_g = \frac{RT}{V_m - b} - \frac{\alpha\alpha}{V_m^2 + 2bV_m - b^2} \quad (1)$$

where P_g represents the pressure of methane gas, R is the gas constant, T is the temperature of the sample, V_m is given by V_g/n_g and represents the molar volume of the gas, where n_g represents the mole number of the gas, $\alpha = 0.45724R^2T_c^2/P_c$, $b = 0.077820RT_c/P_c$, where T_c (190.6 K) and P_c (4.656 MPa) represent the critical temperature and pressure of methane, respectively, and $\alpha = (1 + 0.37464 + 1.54226\omega - 0.26992\omega^2)(1-T_r^{0.5})^2$, where ω is the acentric factor of methane (0.0108) and T_r is given by T/T_c , which represents the reduced temperature. The mole number of the consumed methane gas, i.e., the mole number of the formed natural gas hydrates, was eventually acquired, and the saturation was determined as 20.1%. This agreed well with the image reconstruction method, verifying that 3D reconstruction using CT images is an effective method for observing and analyzing natural gas hydrate-bearing sediments. Additionally, the spatial distributions of each component, including natural gas hydrates, free gas, and water, are shown in panels b, c, and d of Figure 4, respectively. The low water volume in the free gas layer and low solubility and diffusion of methane gas into water lead to the low saturation of natural gas hydrates at the top and bottom of the sediments, as shown in Figure 4b. Large amounts of water were shown to accumulate in the lower part of the sample. As shown in Figure 4c, the existence of free gas in the pores was non-uniform and there was an absence of methane gas in some lower areas. This prevented contact between the gas and water and, consequently, prevented the formation of natural gas hydrates. The spatial occurrence of the hydrate phase within the pores is shown in Figure 5. This further verifies that natural gas hydrates formed and floated within the pore spaces rather than cementing the grain surfaces. Figure 5c illustrates the gray-scale distribution on the segment AD in Figure 5b. Clear spaces existed between the natural gas hydrates and the grains where the water layer coated the sands. However, despite no direct contact, natural gas hydrates within the pores might act as a skeleton to restrict the further motion of surrounding grains to occupy the pores, thereby affecting the mechanical properties of the natural gas hydrate-bearing sediments.

The nucleation character governs the occurrence model and microstructural distribution of natural gas hydrates within the pores. The crystallization of hydrates can occur in three patterns based on the existing theory: homogeneous nucleation as spherical clusters and heterogeneous nucleation as cap-shaped or lens-shaped clusters, as shown in panels a, b, and c of Figure 6, respectively.^{48,49} In a porous system, because of the existence of gas and sands, hydrates are considered to nucleate heterogeneously.^{22,50} The work (W) to form n units of hydrates can be expressed by the following equation:⁴⁸

$$W = -n\Delta\mu + cv_h^{2/3}\sigma_{ef}n^{2/3} \quad (2)$$

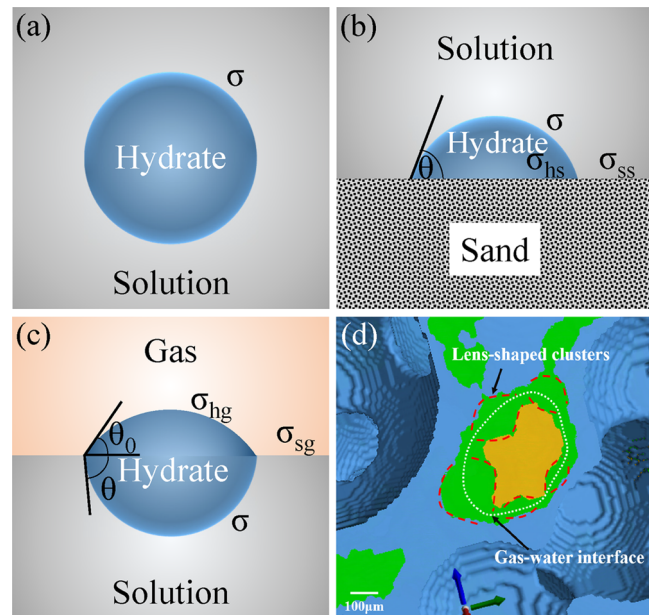


Figure 6. (a–c) Schematic of different types of hydrate nucleation⁴⁹ and (d) lens-shaped hydrate clusters in our study. θ and θ_0 are the contact angles of different surfaces, and σ represents the specific surface energy of different interfaces. Subscripts h, g, and s are hydrate, gas, and sand or solution, respectively.

where c is a numerical shape factor, v_h is the volume of a hydrate unit, and σ_{ef} is the effective specific surface energy. $\Delta\mu$ is the supersaturation, which is given by $kT \ln[\varphi(P,T)P/\varphi(P_e,T)P_e] + \Delta v_e(P - P_e)$,⁴⁹ where k represents the Boltzmann constant, P and T represent the specific pressure and temperature of the system, respectively, φ is the fugacity coefficient, P_e is the hydrate/solution/gas equilibrium pressure, and $\Delta v_e = n_w v_w - v_h$, where n_w is the hydration number of gas hydrates and v_w is the volume of a water molecule in the solution.^{12,51} Natural gas hydrates are observed to form at the interface between gas and water, which can be attributed to the relatively higher supersaturation ($\Delta\mu$) in the thin water layer at the interface.^{49,50} Therefore, the work needed to form hydrate clusters is lower at the gas–solution interface, where natural gas hydrates nucleate preferentially. This agrees with our visualizations, as shown in Figure 6d. The white circle is considered the original gas–water interface, where hydrate clusters were initiated and accumulated. The red curves describe the lens shape of the clusters. As the clusters grew larger, they were joined together, preventing further contacts between gases and water. The local reaction was completed when no gas–water interface existed. Therefore, natural gas hydrates are indicated to form at the gas–water interface, with lens-shaped clusters floating within the pores.

In this work, a microfocus X-ray CT experimental system was established to directly observe the microstructure and occurrence of natural gas hydrates within porous media. The spatial distribution of each component within the pores, including natural gas hydrates, water, and free gas, was clearly identified. It indicated that both the migration of gas and water during hydrate formation and the nucleating site of natural gas hydrates were random. In addition, natural gas hydrates were observed to occur mainly within pore spaces without contacting the adjacent grains. Therefore, the occurrence model of natural gas hydrates within sediments was most likely the floating model. There existed a water layer coating the surface of grains.

Natural gas hydrates are considered to nucleate heterogeneously as lens-shaped clusters at the gas–water interface. Moreover, the low solubility and diffusivity of methane gas into pore water and low water saturation in the free gas layer primarily affected the formation of natural gas hydrates with high saturation. The porosity and hydrate saturation obtained using 3D reconstructions agreed well with the conventional methods, indicating that X-ray CT can be effective in the microstructural investigation of natural gas hydrate-bearing sediments. These findings could have implications regarding the transmission and attenuation of seismic waves in natural gas hydrate reserves during both hydrate exploration and resource assessment and investigations on continental slope stability during gas production.

AUTHOR INFORMATION

Corresponding Authors

*J. Zhao. E-mail: jfzhao@dlut.edu.cn.

*Y. Song. E-mail: songyc@dlut.edu.cn.

Notes

The authors declare no competing financial interest.

ACKNOWLEDGMENTS

This study has been supported by the National Science and Technology Major Project of China (Grant 2011ZX05026-004-07), the National High Technology Research and Development Program of China “863 Program” (Grant 2013AA09250302), the Natural Science Foundation of China (Grants 51227005, 51376034, and 51276028), and the China Postdoctoral Science Foundation (Grant 2014M560206).

REFERENCES

- Sloan, E. D. Fundamental principles and applications of natural gas hydrates. *Nature* **2003**, *426*, 353–359.
- Boswell, R.; Collett, T. S. Current perspectives on gas hydrate resources. *Energy Environ. Sci.* **2011**, *4* (4), 1206–1215.
- Koh, C. A. Towards a fundamental understanding of natural gas hydrates. *Chem. Soc. Rev.* **2002**, *31* (3), 157–167.
- Koh, C. A.; Sum, A. K.; Sloan, E. D. State of the art: natural gas hydrates as a natural resource. *J. Nat. Gas Sci. Eng.* **2012**, *8*, 132–138.
- Song, Y.; Yang, L.; Zhao, J.; Liu, W.; Yang, M.; Li, Y.; Liu, Y.; Li, Q. The status of natural gas hydrate research in China: A review. *Renewable Sustainable Energy Rev.* **2014**, *31*, 778–791.
- Du, J.; Li, H.; Wang, L. Effects of ionic surfactants on methane hydrate formation kinetics in a static system. *Adv. Powder Technol.* **2014**, *25* (4), 1227–1233.
- Du, J.; Wang, L.; Liang, D.; Li, D. Phase equilibria and dissociation enthalpies of hydrogen semi-clathrate hydrate with tetrabutyl ammonium nitrate. *J. Chem. Eng. Data* **2012**, *57* (2), 603–609.
- Jones, K. W.; Kerkar, P. B.; Mahajan, D.; Lindquist, W. B.; Feng, H. Microstructure of natural hydrate host sediments. *Nucl. Instrum. Methods Phys. Res., Sect. B* **2007**, *261* (1–2), 504–507.
- Delahaye, A.; Fournaison, L.; Guilpart, J. Characterisation of ice and THF hydrate slurry crystal size distribution by microscopic observation method. *Int. J. Refrig.* **2010**, *33* (8), 1639–1647.
- Yamamoto, K. Methane hydrate bearing sediments: A new subject of geomechanics. *Proceedings of the 12th International Conference of International Association for Computer Methods and Advances in Geomechanics (IACMAG)*; Goa, India, Oct 1–6, 2008; pp 1188–1196.
- Max, M. D. *Natural Gas Hydrate in Oceanic and Permafrost Environments*; Springer: New York, 2003; Vol. 5.
- Sloan, E. D., Jr.; Koh, C. *Clathrate Hydrates of Natural Gases*; CRC Press: Boca Raton, FL, 2007.
- Huang, J.; Bellefleur, G.; Milkereit, B. Seismic modeling of multidimensional heterogeneity scales of Mallik gas hydrate reservoirs, Northwest Territories of Canada. *J. Geophys. Res.* **2009**, DOI: [10.1029/2008JB006172](https://doi.org/10.1029/2008JB006172).
- Matsuhashima, J. Seismic wave attenuation in methane hydrate-bearing sediments: Vertical seismic profiling data from the Nankai Trough exploratory well, offshore Tokai, central Japan. *J. Geophys. Res.* **2006**, DOI: [10.1029/2005JB004031](https://doi.org/10.1029/2005JB004031).
- Bellefleur, G.; Riedel, M.; Brent, T. Seismic characterization and continuity analysis of gas-hydrate horizons near Mallik research wells, Mackenzie Delta, Canada. *Leading Edge* **2006**, *25* (5), 599–604.
- Dvorkin, J.; Uden, R. Seismic wave attenuation in a methane hydrate reservoir. *Leading Edge* **2004**, *23* (8), 730–732.
- Kleinberg, R.; Flaum, C.; Griffin, D.; Brewer, P.; Malby, G.; Peltzer, E.; Yesinowski, J. Deep sea NMR: Methane hydrate growth habit in porous media and its relationship to hydraulic permeability, deposit accumulation, and submarine slope stability. *J. Geophys. Res.* **2003**, DOI: [10.1029/2003JB002389](https://doi.org/10.1029/2003JB002389).
- Kerkar, P.; Jones, K. W.; Kleinberg, R.; Lindquist, W. B.; Tomov, S.; Feng, H.; Mahajan, D. Direct observations of three dimensional growth of hydrates hosted in porous media. *Appl. Phys. Lett.* **2009**, *95* (2), 024102.
- Uchida, T.; Dallimore, S.; Mikami, J. Occurrences of Natural Gas Hydrates beneath the Permafrost Zone in Mackenzie Delta: Visual and X-ray CT Imagery. *Ann. N. Y. Acad. Sci.* **2000**, *912* (1), 1021–1033.
- Klaproth, A.; Techmer, K.; Klapp, S.; Murshed, M.; Kuhs, W. Microstructure of gas hydrates in porous media. *Spec. Publ.—R. Soc. Chem.* **2006**, *311*, 321.
- Xue, K.; Zhao, J.; Song, Y.; Liu, W.; Lam, W.; Zhu, Y.; Liu, Y.; Cheng, C.; Liu, D. Direct observation of thf hydrate formation in porous microstructure using magnetic resonance imaging. *Energies* **2012**, *5* (4), 898–910.
- Song, Y.; Xue, K.; Zhao, J.; Lam, W.; Cheng, C.; Yang, M.; Zhang, Y.; Wang, D.; Liu, W.; Liu, Y. In situ observation of hydrate growth habit in porous media using magnetic resonance imaging. *EPL* **2013**, *101* (3), 36004.
- Leaist, D.; Murray, J.; Post, M.; Davidson, D. Enthalpies of decomposition and heat capacities of ethylene oxide and tetrahydrofuran hydrates. *J. Phys. Chem.* **1982**, *86* (21), 4175–4178.
- Tse, J. S.; White, M. A. Origin of glassy crystalline behavior in the thermal properties of clathrate hydrates: a thermal conductivity study of tetrahydrofuran hydrate. *J. Phys. Chem.* **1988**, *92* (17), 5006–5011.
- Yun, T. S.; Santamarina, J. C.; Ruppel, C. Mechanical properties of sand, silt, and clay containing tetrahydrofuran hydrate. *J. Geophys. Res.* **2007**, DOI: [10.1029/2006JB004484](https://doi.org/10.1029/2006JB004484).
- Seol, Y.; Kneafsey, T. J. X-ray computed-tomography observations of water flow through anisotropic methane hydrate-bearing sand. *J. Pet. Sci. Eng.* **2009**, *66* (3), 121–132.
- Rees, E. V.; Priest, J. A.; Clayton, C. R. The structure of methane gas hydrate bearing sediments from the Krishna–Godavari Basin as seen from Micro-CT scanning. *Mar. Pet. Geol.* **2011**, *28* (7), 1283–1293.
- Ohno, H.; Narita, H.; Nagao, J. Different modes of gas hydrate dissociation to ice observed by microfocus X-ray computed tomography. *J. Phys. Chem. Lett.* **2011**, *2* (3), 201–205.
- Abegg, F.; Bohrmann, G.; Freitag, J.; Kuhs, W. Fabric of gas hydrate in sediments from Hydrate Ridge—results from ODP Leg 204 samples. *Geo-Mar. Lett.* **2007**, *27* (2–4), 269–277.
- Jin, Y.; Konno, Y.; Nagao, J. Pressurized subsampling system for pressurized gas-hydrate-bearing sediment: Microscale imaging using X-ray computed tomography. *Rev. Sci. Instrum.* **2014**, *85* (9), 094502.
- Ta, X. H.; Yun, T. S.; Muhunthan, B.; Kwon, T. H. Observations of pore-scale growth patterns of carbon dioxide hydrate using X-ray computed microtomography. *Geochem., Geophys., Geosyst.* **2015**, *16* (3), 912–924.

- (32) Hu, G.; Li, C.; Ye, Y.; Liu, C.; Zhang, J.; Diao, S. Observation of gas hydrate distribution in sediment pore space. *Chin. J. Geophys.* **2014**, *57* (5), 1675–1682.
- (33) Kneafsey, T. J.; Tomutsa, L.; Moridis, G. J.; Seol, Y.; Freifeld, B. M.; Taylor, C. E.; Gupta, A. Methane hydrate formation and dissociation in a partially saturated core-scale sand sample. *J. Pet. Sci. Eng.* **2007**, *56* (1), 108–126.
- (34) Waite, W. F.; Kneafsey, T. J.; Winters, W. J.; Mason, D. H. Physical property changes in hydrate-bearing sediment due to depressurization and subsequent repressurization. *J. Geophys. Res.: Solid Earth* **2008**, *113* (B7), B07102.
- (35) Waite, W. F.; Santamarina, J. C.; Cortes, D. D.; Dugan, B.; Espinoza, D. N.; Germaine, J.; Jang, J.; Jung, J. W.; Kneafsey, T. J.; Shin, H.; Soga, K.; Winters, W. J.; Yun, T. S. Physical properties of hydrate-bearing sediments. *Rev. Geophys.* **2009**, *47* (4), RG4003.
- (36) Mikami, J.; Masuda, Y.; Uchida, T.; Satoh, T.; Takeda, H. Dissociation of Natural Gas Hydrates Observed by X-ray CT Scanner. *Ann. N. Y. Acad. Sci.* **2000**, *912* (1), 1011–1020.
- (37) Jin, S.; Takeya, S.; Hayashi, J.; Nagao, J.; Kamata, Y.; Ebinuma, T.; Narita, H. Structure analyses of artificial methane hydrate sediments by microfocus X-ray computed tomography. *Jpn. J. Appl. Phys.* **2004**, *43* (8), 5673–5675.
- (38) Jin, S.; Nagao, J.; Takeya, S.; Jin, Y.; Hayashi, J.; Kamata, Y.; Ebinuma, T.; Narita, H. Structural investigation of methane hydrate sediments by microfocus X-ray computed tomography technique under high-pressure conditions. *Jpn. J. Appl. Phys.* **2006**, *45* (7L), L714.
- (39) Klapp, S. A.; Enzmann, F.; Walz, P.; Huthwelker, T.; Tuckermann, J. r.; Schwarz, J.-O.; Pape, T.; Peltzer, E. T.; Mokso, R.; Wangner, D. Microstructure characteristics during hydrate formation and dissociation revealed by X-ray tomographic microscopy. *Geo-Mar. Lett.* **2012**, *32* (5–6), 555–562.
- (40) Murshed, M. M.; Klapp, S. A.; Enzmann, F.; Szeder, T.; Huthwelker, T.; Stampanoni, M.; Marone, F.; Hintermüller, C.; Bohrmann, G.; Kuhs, W. F. Natural gas hydrate investigations by synchrotron radiation X-ray cryo-tomographic microscopy (SRXCTM). *Geophys. Res. Lett.* **2008**, DOI: [10.1029/2008GL035460](https://doi.org/10.1029/2008GL035460).
- (41) Zhong, Y.; Rogers, R. Surfactant effects on gas hydrate formation. *Chem. Eng. Sci.* **2000**, *55* (19), 4175–4187.
- (42) Buffett, B.; Zatsepina, O. Y. Formation of gas hydrate from dissolved gas in natural porous media. *Mar. Geol.* **2000**, *164* (1), 69–77.
- (43) Zhang, Y.; Wang, Q. Application of Software VGStudio MAX 2.0 in 3D Reconstruction of Industrial Computed Tomography Images. *Metrol. Meas. Technol.* **2011**, *5*, 011.
- (44) Sato, M.; Takeya, S.; Nagao, J.; Jin, S.; Kamata, Y.; Minagawa, H.; Ebinuma, T.; Narita, H. Distribution of hydrate saturation ratios in artificial methane hydrate sediments measured by high-speed X-ray computerized tomography. *Jpn. J. Appl. Phys.* **2005**, *44* (1R), 473.
- (45) Peng, D.-Y.; Robinson, D. B. A new two-constant equation of state. *Ind. Eng. Chem. Fundam.* **1976**, *15* (1), 59–64.
- (46) Cismonti, M.; Mollerup, J. Development and application of a three-parameter RK–PR equation of state. *Fluid Phase Equilib.* **2005**, *232* (1), 74–89.
- (47) Picard, D.; Bishnoi, P. The importance of real-fluid behavior and nonisentropic effects in modeling decompression characteristics of pipeline fluids for application in ductile fracture propagation analysis. *Can. J. Chem. Eng.* **1988**, *66* (1), 3–12.
- (48) Kashchiev, D. *Nucleation: Basic Theory with Applications*. Butterworth-Heinemann: Boston, MA, 2000; pp 55–67.
- (49) Kashchiev, D.; Firoozabadi, A. Nucleation of gas hydrates. *J. Cryst. Growth* **2002**, *243* (3), 476–489.
- (50) Englezos, P.; Kalogerakis, N.; Dholabhai, P.; Bishnoi, P. Kinetics of formation of methane and ethane gas hydrates. *Chem. Eng. Sci.* **1987**, *42* (11), 2647–2658.
- (51) Firoozabadi, A. *Thermodynamics of Hydrocarbon Reservoirs*; McGraw-Hill: New York, 1999.